Nano Research

Open Access

Research Article

Defect engineering for achieving multi-electrons storage in VS_4 to enhance magnesium storage performance

Jiankang Chen, Guofeng Wang, Bing Sun, Yu Zhang, Maoyuan Li, Lei Wang, Guicun Li, Alan Meng, Shiqi Ding ✉, and Zhenjiang Li ✉

College of Materials Science and Engineering, Key Laboratory of Optic-electric Sensing and Analytical Chemistry for Life Science, MOE, Shandong Key Laboratory of Biochemical Analysis, College of Chemistry and Molecular Engineering, Qingdao University of Science and Technology, Qingdao 266042, China

Cite this article: *Nano Research*, **2025**, *18*, 94907393. https://doi.org/10.26599/NR.2025.94907393

ABSTRACT: Defect engineering acts as an efficiency method to modulate the microstructure and electronic structure of cathode for rechargeable magnesium batteries (RMBs). Owing to rich sulfur (S) vacancies tunes the electronic structure of VS_4 with rich S vacancies (V_S-VS_4), the lower oxidation state of V^{3+} is induced for achieving the V^{3+}/V^{4+} and V^{4+}/V^{5+} multi-electrons reaction for Mg^{2+} storage. Amorphous structure is also constructed in V_S-VS_4 by chemical vapor deposition (CVD) method under the high temperature for providing fast magnesium ions (Mg^{2+}) diffusion channels and expanding inner stress release space to balance the structural stability of multi-electrons reaction process. The simple defect engineering realizes the stable multi-electrons reaction in V_S-VS_4 for enhancing its Mg^{2+} storage performance with higher specific capacity (158.6 mAh·g^{-1} at 50 mA·g^{-1}), stable cycling performance (capacity retention ratio of 72.7% after 3600 cycles) and the superior rate capability. This work provides electrode designing guidance for achieving stable multi-electrons to fully utilize the bivalent property of multivalence metal batteries.

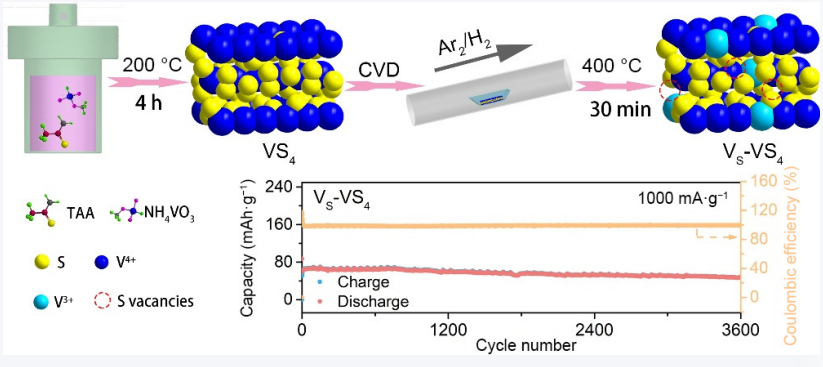

KEYWORDS: defect engineering, multi-electrons reaction, VS_4, cathode, rechargeable magnesium batteries (RMBs)

1 Introduction

There is an urgent need to expedite the development of clean and sustainable energy due to the pervasive global environmental contamination and substantial depletion of non-renewable energy reserves [1]. Electrochemical energy storage technologies have emerged as the essential technology for meeting such challenges [2], rechargeable magnesium batteries (RMBs) with Mg metal as anode have received tremendous attentions owing to high volumetric capacity (3833 mAh·cm^{-3}), low reduction potential (−2.37 V vs. SHE) and earth-abundant (≈ 1000 times more than Li) of Mg metal [3–5]. Although the bivalent property of Mg^{2+} endows the above advantages for RMBs, most cathode would not to utilize its bivalent property due to the less amount of electrons participating in Mg^{2+} storage process [6]. Therefore, in order to meet the acquirement of the application of RMBs, there is great demand to fully utilize the bivalent property of Mg^{2+} by cathode designing.

Cathode based on multi-electrons reaction is an effective path to utilize the bivalent property of Mg^{2+}, however, it is difficult to achieve in typical intercalation-type cathode [7]. As for VS_4 cathode, it owns the unique linear-chain structure composed by V^{4+} and S_2^{2-} with the larger interplanar spacing of 0.56 nm for Mg^{2+} diffusion and adsorption [8]. When applied VS_4 as cathode in RMBs, previous literatures found that the Mg^{2+} storage process for VS_4 is the oxidation of V accompanied by the reduction of S [9], in other words, V^{4+} would be oxidated to V^{5+} during Mg^{2+} insertion process accompanied by the reduction of S_2^{2-} to S^{2-}, which is confirmed by both theoretically and experimentally [10]. Inspired by the change law of VS_4 during Mg^{2+} storage process, the change of electronic structure around V atoms for constructing the lower oxidation state

Received: March 6, 2025; **Revised:** March 19, 2025
Accepted: March 19, 2025

✉Address correspondence to Shiqi Ding, zaddmn1830@163.com; Zhenjiang Li, zhenjiangli@qust.edu.cn

of V including V^{3+} may be the valid way to achieve the V^{3+}/V^{4+} and V^{4+}/V^{5+} multi-electrons reaction in VS_4 for the superior Mg^{2+} storage performance.

However, it is well known that the increased electrons amount involved in Mg^{2+} storage process, the more furious of Mg^{2+} storage reaction, leading to the drastic change of cathode structure for influencing the Mg^{2+} storage stability [11]. Defect engineering is regarded as simple and common method to modulate the microstructure to tune the Mg^{2+} diffusion channels [12]. Besides that, the defect sites could act as active sites to adsorb more Mg^{2+} to enhance specific capacity, which could also assist the multi-electrons storage process [13]. In recent years, researchers have focused on defect engineering on cathode designment, Chen et al. introduce O vacancies in V_2O_5 to improve Mg^{2+} migration kinetics, structural stability and electronic conductivity, making V_2O_5 with rich O vacancies delivers the higher specific capacity within 850 cycles [14]. Jiang et al. introduced rich S vacancies in VS_4 for alleviating the sluggish kinetics, irreversible structgural change, short cycle life and low capacity of RMBs [15]. Therefore, defect engineering would enhance the Mg^{2+} storage stability during the drastic multi-electrons storage process. As reported in previous literatures, defect engineering is also important to modify the surface chemistry of cathode [16]. When introducing rich vacancies in VS_4 cathode, the charge distribution around V and S atoms are changing, which is beneficial to modulate the oxidation state of V, therefore, it is expected to achieve the stable multi-electrons reaction process in VS_4 for Mg^{2+} storage, which has not been reported in other literatures.

In this work, defect engineering including amorphous structure and rich S vacancies are constructed in VS_4 (V_S-VS_4) via chemical vapour deposition (CVD) method under the H_2 atmosphere. The reduction characteristic of H_2 would take off anion from VS_4 to form rich S vacancies, besides that, the high-temperature calcine treatment make VS_4 have the metastable structure, which owns the amorphous structure. Such amorphous structure would provide more active sites to adsorb more Mg^{2+} to enhance specific capacity, and the isotropy property for amorphous structure would facilitate Mg^{2+} diffusion to enhance Mg^{2+} storage kinetics. Rich S vacancies modulate electronic structure in V_S-VS_4 to modulate the lower oxidation state of V^{3+}, which achieve the V^{3+}/V^{4+} and V^{4+}/V^{5+} multi-electrons reaction process in V_S-VS_4 for boosting fast Mg^{2+} diffusion kinetics and enhancing specific capacity. Benefiting from the defect engineering, V_S-VS_4 delivers the longer cycling life of 3600 cycles with capacity retention ratio of 72.7%, higher specific capacity of 158.6 $mAh{\cdot}g^{-1}$ at 50 $mA{\cdot}g^{-1}$, and the superior rate capability. The defect engineering for guiding cathode for achieving multi-electrons reaction for fully utilizing the multi-valence properties in.

2 Experimental

2.1 Materials synthesis

All the chemicals and materials including ammonium metavanadate (NH_4VO_3) and thioacetamide (TAA) are of analytical grade and were used without further purification, which were purchased from Ahanghai Aladdin Biochemical Technology Co., Ltd and Shanghai Macklin Biochemical Co., Ltd, respectively. VS_4 was first synthesized via solvothermal method according to previous reported literature [17]. Some as-prepared VS_4 were dispersed in the porcelain boat and treated at 400 °C for 30 min under the Ar_2/H_2 mixture atmosphere to introduce anionic (S) vacancies, after cooling down to room temperature spontaneously, the obtained product was named as V_S-VS_4.

2.2 Materials characterizations

Structural information was analyzed by powder XRD on Bruker D8 Advance with Cu Kα radiation, as well as transmission electron microscope (TEM, JEOL JEM-F200). The chemical information was obtained by X-ray photoelectron spectroscopy (XPS), which was conducted on Thermo Fisher ESCALAB 250Xi with Al Kα source. Scanning electron microscope (SEM, Hitachi SU8010) was used to obtain the morphology information. Rich V and S vacancies were analyzed by electron paramagnetic resonance (EPR, Bruker EMXPLUS).

2.3 Battery fabrication and electrochemical characterizations

The cathode for VS_4 and V_S-VS_4 was fabricated by casting a slurry composed of as-synthesized active materials, super P and PVDF with weight ratio of 6:3:1 in N-methyl-2-pyrrolidone on carbon paper current collector. The as-prepared cathode was assembled with Mg foil, 100 μL of (0.4 M $(PhMgCl)_2$-$AlCl_3$/tetrahydrofuran (APC/THF)) and Whatman glass fiber as anode, electrolyte and separator, respectively. The assembled RMBs were tested by cyclic voltammetry (CV) measurements and electrochemical impedance spectra (EIS), which are conducted on CHI660E electrochemistry workstation. The scan rate for CV tests was in range from 0.1 to 0.8 $mV{\cdot}s^{-1}$, and EIS is obtained with frequency range from 0.01 Hz to 100 KHz. The cycling performance, rate capability and the galvanostatic intermittent titration technique (GITT) of RMBs were tested on LAND CT-2001A instrument. The voltage window was in range of 0.2 to 2.1 V with current density from 50 to 1000 $mA{\cdot}g^{-1}$.

3 Results and discussion

Establishment mechanism for multi-category defects in V_S-VS_4 structure is shown in Fig. 1(a), VS_4 is firstly fabricated by solvothermal method. When calcining VS_4 under the Ar_2/H_2 atmosphere, the reductive property of H_2 atmosphere would cause rich S vacancies in V_S-VS_4 structure. Rich S vacancies would alter the charge distribution to construct the lower oxidation state of V^{3+} in V_S-VS_4, which is expected to achieve the multi-electrons reaction during Mg^{2+} storage process. At the same time, rich S vacancies would increase the adsorption sites for Mg^{2+} reaction as well as enhance the adsorption intensity with Mg^{2+} to improve the specific capacity. Besides that, the calcining treatment at the higher temperature would cause the fast diffusion of atoms, therefore, the amorphous structure is also established in V_S-VS_4, which is also beneficial for facilitating Mg^{2+} diffusion to enhance Mg^{2+} storage kinetics and maintain Mg^{2+} storage stability.

To further detect its crystal and phase structure, XRD patterns of VS_4 and V_S-VS_4 are shown in Fig. 1(b), the diffraction peaks of VS_4 correspond to the character peaks of monoclinic VS_4 (PDF #72-1294). However, there are no obvious diffraction peaks could be observed in V_S-VS_4, revealing that the calcining process would accelerate atoms diffusion to cause structure disorder. Therefore, the amorphous structure is constructed in V_S-VS_4. XPS is carried to investigate the electronic structure of VS_4 and V_S-VS_4. EPR results is further applied to investigate the vacancies concentration in VS_4

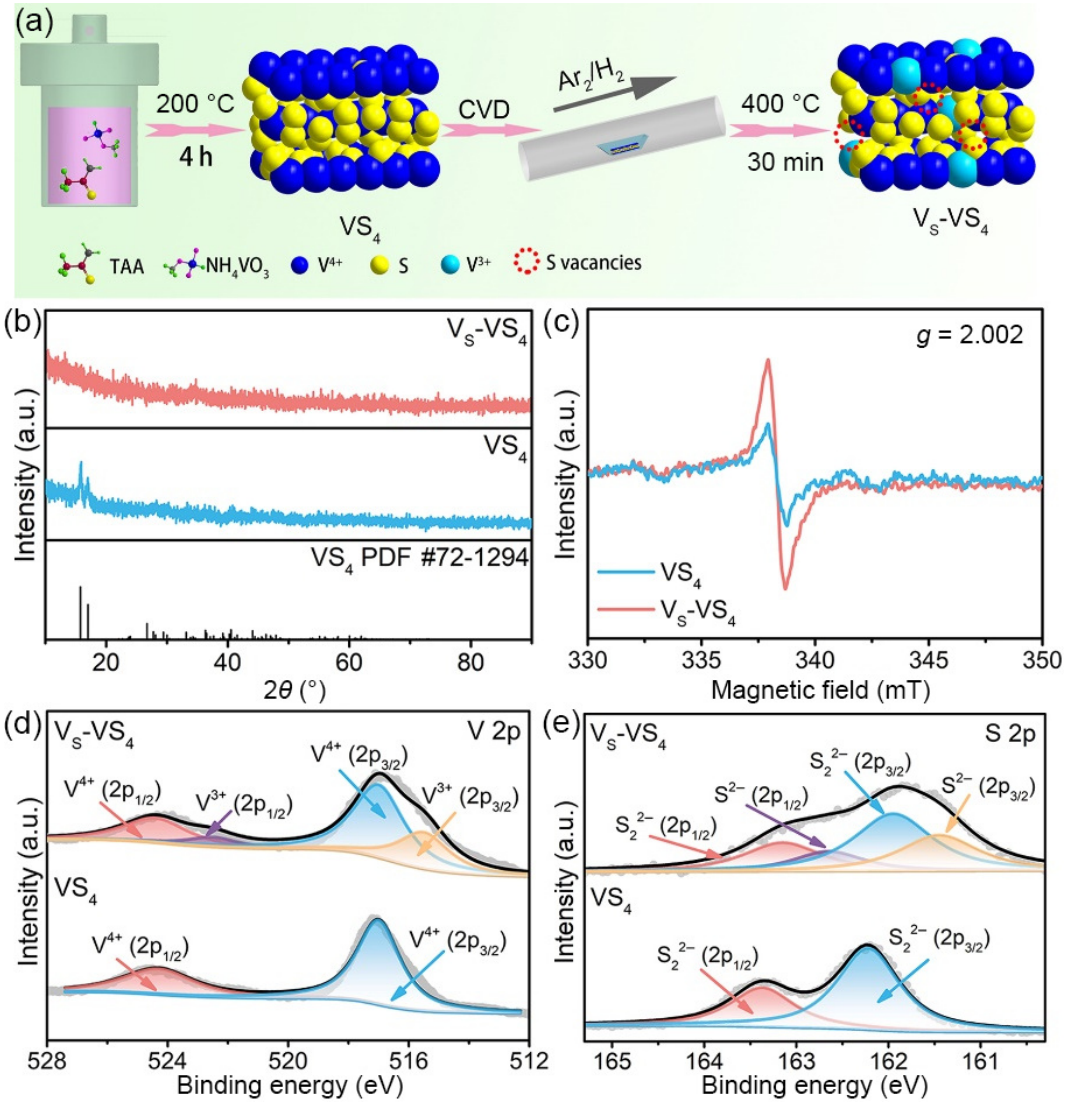

Figure 1 (a) Multi-categories defects formation mechanism in V_S-VS_4. (b) XRD patterns, (c) EPR spectra, (d) V 2p and (e) S 2p XPS spectra of VS_4 and V_S-VS_4.

and V_S-VS_4. As shown in Fig. 1(c), an obvious signal at g = 2.002 could be detected in VS_4 and V_S-VS_4, and the signal intensity of V_S-VS_4 is higher than that of VS_4, indicating that there are rich S vacancies in V_S-VS_4 structure [18].

From XPS survey spectra (Fig. S1 in the Electronic Supplementary Material (ESM)), both V and S elements could be observed in both VS_4 and V_S-VS_4 samples, confirming the formed VS_4 preliminarily. Figure 1(d) shows V 2p high-resolution XPS spectra of VS_4 and V_S-VS_4, the presence of V^{4+} is verified by V $2p_{1/2}$ and V $2p_{3/2}$ at 524.4 and 517.2 eV, respectively [19]. An obvious shift towards the lower binding energy could be observed in V_S-VS_4 (524.3 and 517.1 eV for V $2p_{1/2}$ and V $2p_{3/2}$ of V^{4+}, respectively), which may be caused by the existence of some vacancies in structure [20]. Besides that, the lower oxidation state of V^{3+} could be observed in V_S-VS_4 at binding energy of 522.5 and 515.5 eV [21], indicating that some broken of V–S bond by some S atoms escaping would reduce the coordination number of V, and then reducing its oxidation state. S 2p XPS spectra of VS_4 and V_S-VS_4 are shown in Fig. 1(e), one doublet S $2p_{1/2}$ and S $2p_{3/2}$ at 163.4 eV and 162.3 eV assigned for S_2^{2-} could be detected for VS_4 and V_S-VS_4 samples [22], further confirming the successfully synthesized of VS_4 due to the dimer sulfide (S_2^{2-}) structure for VS_4. However, the position of S_2^{2-} in V_S-VS_4 shifts towards the lower binding energy, which reveals that rich S vacancies exists in V_S-VS_4 structure. Besides that, another one doublet S $2p_{1/2}$ and S $2p_{3/2}$ at 162.7 and 161.5 eV assigned for S^{2-} could be detected for V_S-VS_4, which might be caused by the escaping of some S atoms would break the sulfide (S_2^{2-}) structure [23]. Based on above results, it could be concluded that multi-category defects including the amorphous structure and rich S vacancies are constructed in V_S-VS_4 structure, and the microstructure and oxidation state of V have been modulated by defect engineering.

To further investigate the effect of the existed multi-category defects in V_S-VS_4 on its Mg^{2+} storage performance, series of electrochemical tests are carried out. The CV curves of VS_4 and V_S-VS_4 cathodes during the first five cycles is shown in Fig. S2 in the ESM and Fig. 2(a), the nearly overlapped curves from the second cycle to the fifth cycle suggest the reversible Mg^{2+} storage process. The CV curves of VS_4 and V_S-VS_4 at the fourth cycle shows that two samples own the same peak shape (Fig. 2(b)), suggesting that the intensity of redox peaks for V_S-VS_4 is significant higher than that of VS_4, indicating a faster magnesiation process in V_S-VS_4. The

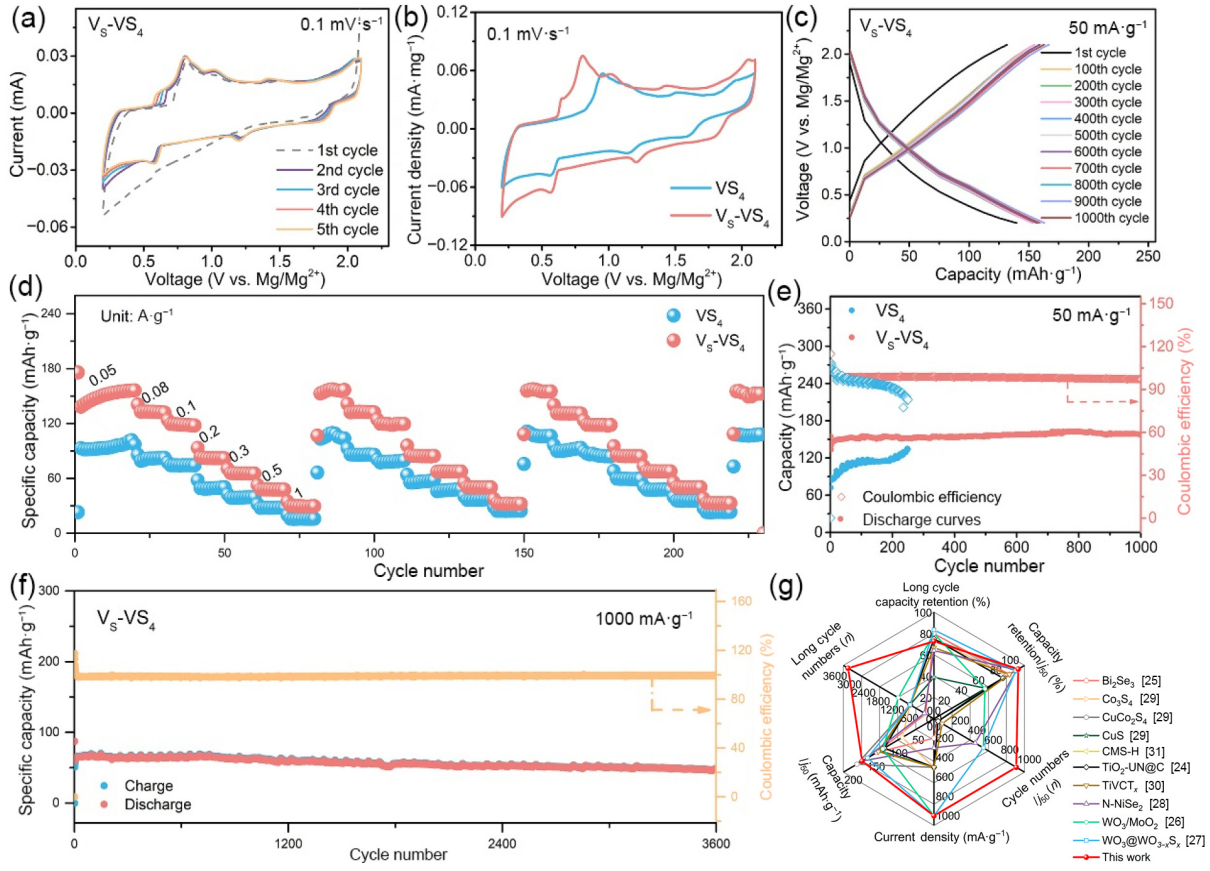

Figure 2 (a) First five CV curves of V_S-VS_4, (b) the fourth cycle for CV curves, (c) the galvanostatic charge–discharge profiles of V_S-VS_4 at various cycles, (d) rate capability of VS_4 and V_S-VS_4, and (e) cycling performance of VS_4 and V_S-VS_4. (f) Cycling performance of V_S-VS_4 at 1000 mA·g^{-1}. (g) Comparison electrochemical performance of V_S-VS_4 and cathodes in reported literatures.

gaovanostatic charge-discharge results of V_S-VS_4 cathode at various cycles from the first cycle to the 1000th cycle are shown in Fig. 2(c), V_S-VS_4 shows a stable specific capacity of about 153.2 mAh·g^{-1}, delivering the superior cycling stability, which could be ascribed to the enough space in structure with both amorphous structure and rich S vacancies would timely release the inner stress generated during the cycling process. Figure 2(d) shows the rate performance of VS_4 and V_S-VS_4 cathodes, the V_S-VS_4 cathode shows considerable reversible capacities of 156.2, 132.5, 118.7, 82, 65.3, 47.8 and 29.4 mAh·g^{-1} at 0.05, 0.08, 0.1, 0.2, 0.3, 0.5 and 1 A·g^{-1}, respectively. After the repeated change of current density, the specific capacity at each current density would not decrease, and when the current density is resorted to 0.05 A·g^{-1}, V_S-VS_4 cathode could still deliver the higher specific capacity of 155.5 mAh·g^{-1}, revealing the superior reversible magnesiation/demagnesiation property and superior reaction kinetics of V_S-VS_4 cathode. However, the specific capacity for VS_4 cathodes at the same changing of current densities are lower than V_S-VS_4, which are 100.4, 81.8, 74.3, 49.1, 39, 27.7 and 15.8 mAh·g^{-1} at 0.05, 0.08, 0.1, 0.2, 0.3, 0.5 and 1 A·g^{-1}, respectively. The superior rate performance of V_S-VS_4 could be attributed to the multi-category defects including the amorphous structure and rich S vacancies would enhance the diffusion kinetics of Mg^{2+}. From cycling performance of VS_4 and V_S-VS_4 (Fig. 2(e)), it could be observed that V_S-VS_4 presents the stable cycling performance with cycling number of 1000 cycles and reversible specific capacity of 158.6 mAh·g^{-1}. In comparison, VS_4 could only cycle for 200 cycles with the lower specific capacity of 117.5 mAh·g^{-1} without defect engineering. At presented in Fig. 2(f), cycling performance of V_S-VS_4 tested at the higher current density of 1000 mA·g^{-1} shows the higher capacity retention ratio of 72.7% after 3600 cycles, which is much higher than reported cathodes in previous literatures (Fig. 2(g)) [24–31]. To further investigate the electrochemical polarization at the interface, the GCD voltage curves of V_S-VS_4 cathode at 1000 mA·g^{-1} is shown in Fig. S3 in the ESM, it could be observed that the curves are almost overlapped at various cycles, suggesting the lower polarization in V_S-VS_4. Therefore, it could be concluded that the multi-category defects engineering could enhance the specific capacity and cycling stability, however, the effect of the enhanced Mg^{2+} storage performance by defect engineering need the further investigation.

EIS before cycling is used to investigate the intrinsic conductivity of VS_4 and V_S-VS_4, as shown in Fig. 3(a), V_S-VS_4 shows the lower charge transfer resistance (R_{ct}), suggesting that the introducing of multi-category defects of amorphous structure as well as rich S vacancies are beneficial to enhance its electronic conductivity. The galvanostatic intermittent titration technique (GITT) tests are carried out to investigate Mg^{2+} diffusion kinetics by calculating the internal resistance and Mg^{2+} diffusion coefficient ($D_{Mg^{2+}}$). Figure 3(b) shows the internal resistance of VS_4 and V_S-VS_4 calculated via GITT results, the internal resistance of V_S-VS_4 is in range of 1.848 to 5.434 Ω, which is lower to that of VS_4 in range of 2.384 to 6.18 Ω. As shown in Fig. 3(c), the $D_{Mg^{2+}}$ values for V_S-VS_4 is in range of 3.6×10^{-15} to 3.02×10^{-12} cm^2·s^{-1} during the cycling process, which is

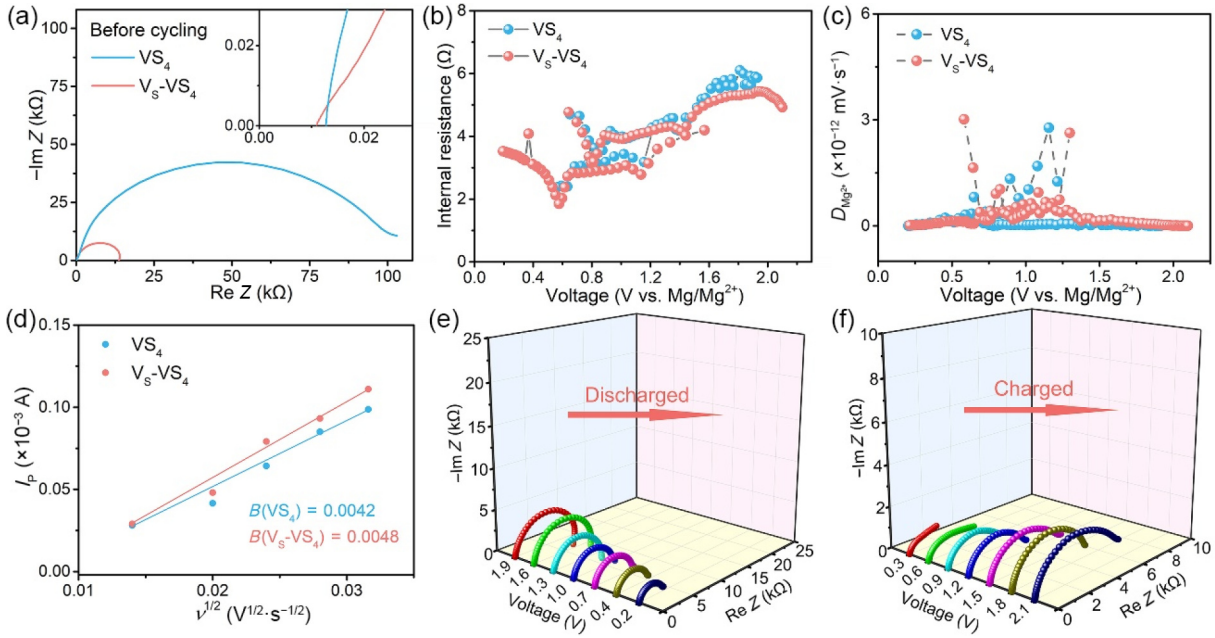

Figure 3 Electrochemical reaction kinetics. (a) EIS spectra of VS_4 and V_S-VS_4 before cycling. (b) Internal resistance and (c) Mg^{2+} diffusion coefficient ($D_{Mg^{2+}}$) of VS_4 and V_S-VS_4. (d) Mg^{2+} diffusion coefficient of VS_4 and V_S-VS_4 evaluated via Randles Sevick equation. EIS spectra of V_S-VS_4 at various discharge (e) and charge (f) voltages.

much larger than that of VS_4 (2.85×10^{-15} to 2.777×10^{-12} $cm^2 \cdot s^{-1}$). A more detailed investigation of the faster kinetics for charging/discharging the V_S-VS_4 cathode than that of VS_4 is performed via CV measurements at various scan rates (Fig. S7 in the ESM). *B* values for VS_4 and V_S-VS_4 are obtained as 0.0042 and 0.0048, respectively (Fig. 3(d)), therefore, the Mg^{2+} diffusion coefficient could be calculated as 8.469×10^{-17} and 1.130×10^{-16} $cm^2 \cdot s^{-1}$, respectively, which also confirms that V_S-VS_4 delivers the faster Mg^{2+} diffusion kinetics after the establishment of the multi-category defects. Therefore, V_S-VS_4 owns the excellent ions diffusion kinetics, which could be mainly attributed to that multi-category defects including amorphous structure and rich S vacancies are conductive to shortening the Mg^{2+} diffusion path and reducing Mg^{2+} diffusion resistance on the one hand, on the other hand, the induced lower oxidation state of V^{3+} may be also benefitted to make more electrons involve in Mg^{2+} storage process for enhancing Mg^{2+} storage kinetics.

To further understand the kinetic characteristics of the electrochemical reaction in V_S-VS_4, *ex situ* EIS tests of V_S-VS_4 are employed at various discharge and charge states. As shown in Figs. 3(e) and 3(f), the R_{ct} values of V_S-VS_4 cathode are gradually decreased during discharging process and increased gradually with the charging continuing, indicating the faster charge transfer rate and reversible Mg^{2+} storage kinetics. Besides that, the R_{ct} values for V_S-VS_4 is decreasing with the cycling number increasing (Fig. S8 in the ESM), suggesting that the construction of multi-category defects boosting the migration of Mg^{2+} at the V_S-VS_4 cathode surface, and consequently benefits to achieve fast kinetics.

The effect of the induced V^{3+} by defect engineering on Mg^{2+} storage mechanism of V_S-VS_4 is investigated by series of *ex situ* characterizations by *ex situ* XPS. Figure 4(a) displays the results of *ex situ* Mg 1s XPS spectra for V_S-VS_4 cathode at fully discharged and charged states. At the pristine state, there is no Mg 1s signal could be observed, and a significant signal assigned as Mg^{2+} could be detected at the fully discharged, indicating the insertion of Mg^{2+} into V_S-VS_4 structure. When further charging to 2.1 V, the intensity of Mg 1s signal is decreased due to the extraction of Mg^{2+} from V_S-VS_4 cathode. However, a weak Mg 1s signal could still be observed due to that some Mg^{2+} remain in V_S-VS_4 structure at the irreversible sites, implying an incomplete demagnesiation reaction, which is in agreement with the result of the difference capacity between the first cycle and following cycles. Compared to the pristine state of V 2p XPS spectra, besides V^{3+} and V^{4+} signals, a pair of addition signals assigned for V^{5+} could be detected at the fully discharge state (Fig. 4(b)), which can be attributed to that partial oxidation of V^{3+} and V^{4+} to V^{5+} when adsorbing Mg^{2+}. After charging to 2.1 V, V^{5+} recovers to V^{4+} and V^{3+}, at the same time, the weakened V^{5+} still exists. Therefore, it could be concluded that the induced V^{3+} in V_S-VS_4 would achieve the V^{3+}/V^{4+} and V^{4+}/V^{5+} multi-electrons reaction process. S 2p XPS spectra (Fig. 4(c)) show that when the V_S-VS_4 cathode is discharged to 0.2 V, the peak of S_2^{2-} becomes weaker, and the intensity of S^{2-} is enhanced. When charging to 2.1 V, the intensity of peaks of S_2^{2-} and S^{2-} return to near their original states. Due to the change of $V^{3+}/V^{4+}/V^{5+}$ oxidation state of V for V_S-VS_4 without the generation of V^0 during magnesium storage process, the magnesium storage mechanism for V_S-VS_4 is the multi-electrons reaction process based on intercalation mechanism, which is illustrated in Fig. 4(d).

Based on above analysis, it could be concluded that the superior Mg^{2+} storage performance of V_S-VS_4 is ascribed to the multi-electrons reaction process, which is induced by defect engineering. The detail reasons could be concluded as following: firstly, defect engineering including rich S vacancies and amorphous structure in V_S-VS_4 structure, which could provide much active sites to adsorb more Mg^{2+} to enhance specific capacity. Secondly, the lower oxidation state of V is induced by defect engineering, which achieve the multi-electrons reaction in V_S-VS_4 for increasing specific capacity. Thirdly, rich S vacancies and amorphous structure would provide more Mg^{2+} diffusion channels as well as release internal stress caused by repeated Mg^{2+} insertion/extraction process, which is beneficial to maintain structure stability and facilitate Mg^{2+} diffusion rate, which could also balance the huge structural change caused by

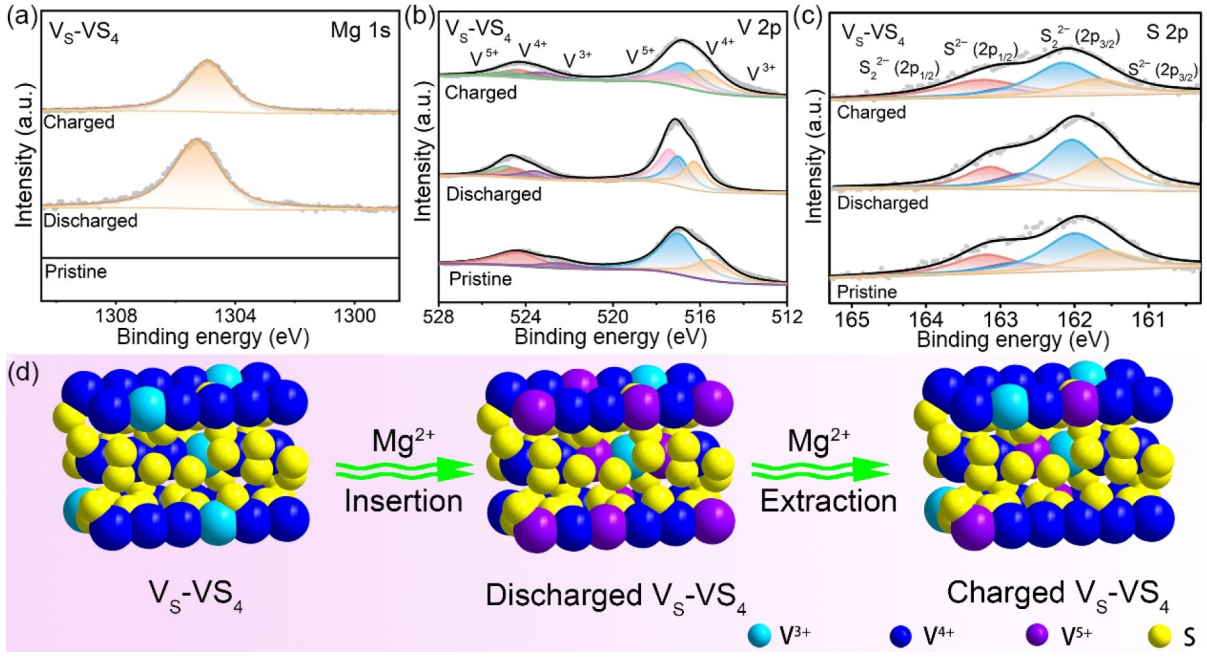

Figure 4 Mg^{2+} storage mechanism analysis. *Ex situ* XPS spectra of Mg 1s (a), V 2p (b) and S 2p (c) for V_S-VS_4 at fully discharged and charged states. (d) Illustration of multi-electrons reaction mechanism of V_S-VS_4.

multi-electrons reaction. Based on the above effects of defect engineering, V_S-VS_4 delivers the superior Mg^{2+} storage performance.

Mg^{2+} storage mechanism in V_S-VS_4 could also be investigated by CV curves tested at various scan rate. As displayed in Figs. 5(a) and 5(b), the fitted *b* values of both anodic and cathodic scans for VS_4 and V_S-VS_4 are in range between 0.5 and 1, indicating that the both surface-controlled and diffusion-controlled process in above cathodes. It is worth noting that *b* values for VS_4 and V_S-VS_4 are gradual increasing, indicating the predominance level of surface-controlled processes in VS_4 is gradual increasing with the constructed defects. The quantitative analysis of surface-controlled and diffusion-controlled process contribution in VS_4 and V_S-VS_4 is shown in Fig. S9 in the ESM, and Figs. 5(c) and 5(d), it could be observed that the surface-controlled process holds the significant current contribution for V_S-VS_4, and the contribution of the surface redox-activity is estimated to be 81.7% at the scan rate of 0.8 $mV \cdot s^{-1}$,

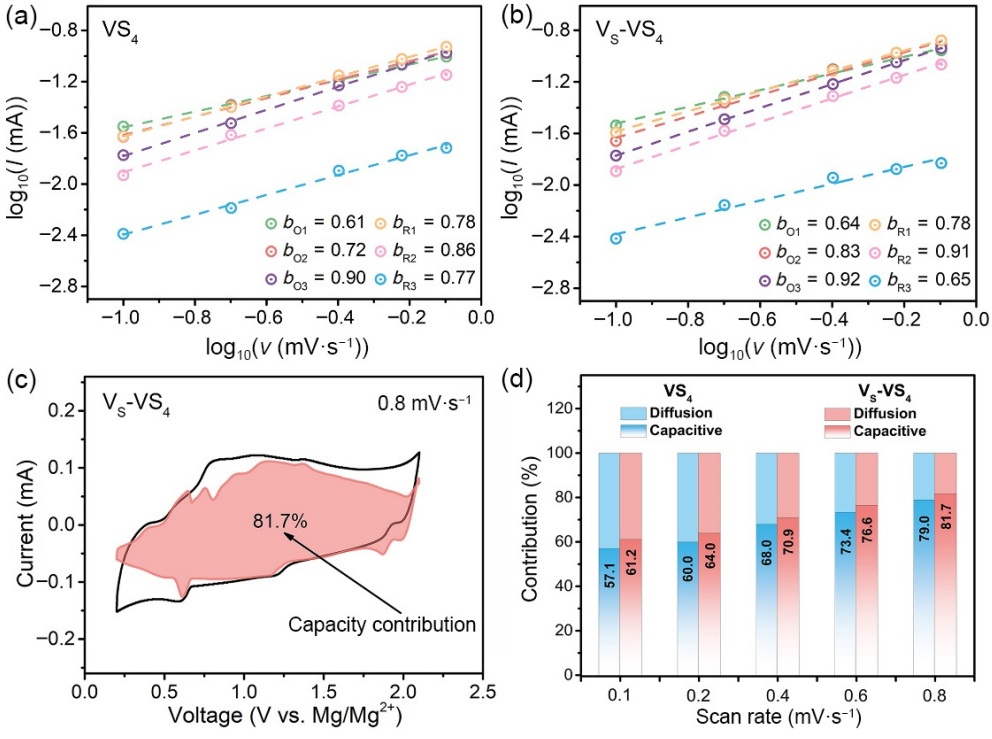

Figure 5 *b* values of (a) VS_4 and (b) V_S-VS_4. (c) Pseudocapacitive contribution for V_S-VS_4 at 0.8 $mV \cdot s^{-1}$. (d) The surface-controlled contributions ratio in VS_4 and V_S-VS_4 at various scan rate.

which is much larger than that of VS_4. It suggests that the rapid redox processes are facilitated by the multi-category defects for V_S-VS_4 via shortening the Mg^{2+} diffusion pathways.

4 Conclusions

In conclusion, defect engineering has applied in V_S-VS_4 for constructing rich S vacancies as well as amorphous structure by CVD method. Rich S vacancies constructed in V_S-VS_4 would not only induce the lower oxidation state of V^{3+} for achieving the V^{3+}/V^{4+} and V^{4+}/V^{5+} multi-electrons reaction for Mg^{2+} storage, but also provide more active sites as multi-electrons reaction sites to increase specific capacity. For S vacancies engineering, V_S-VS_4 is treated under the high temperature, causing the fast diffusion of atoms and then establish the amorphous structure, which is would provide fast Mg^{2+} diffusion channels and release the inner stress timely for maintaining the structural stability to balance the structural change of multi-electrons reaction. Benefitted from the defect engineering, V_S-VS_4 achieve the stable multi-electrons reaction for Mg^{2+} storage in RMBs, which delivers the enhanced specific capacity of 158.6 $mAh{\cdot}g^{-1}$ at 50 $mA{\cdot}g^{-1}$, stable cycling performance with capacity retention ratio of 72.7% after 3600 cycles at 1000 $mA{\cdot}g^{-1}$, and the superior rate capability with reversible specific capacity change when current density increasing to 1000 $mA{\cdot}g^{-1}$. This finding provide the simple method and electronic structure modulation guidance for designing electrodes to achieve the stable multi-electrons reaction in energy storage devices.

Electronic Supplementary Material: Supplementary material (detailed description of GITT and pseudocapacitance-like contribution analysis, XPS survey spectrum, first five CV curves of VS_4, GCD profiles of VS-VS_4 at various cycles, GITT curves, CV curves at various scan rates, EIS spectra, and pseudocapacitive contribution) is available in the online version of this article at https://doi.org/10.26599/NR.2025.94907393.

Data availability

All data needed to support the conclusions in the paper are presented in the manuscript and the ESM. Additional data related to this paper may be requested from the corresponding author upon request.

Acknowledgements

The work reported here was supported by the National Natural Science Foundation of China (Nos. 52072196, 52002200, 52102106, 52202262, 22379081, and 22379080), Major Basic Research Program of Natural Science Foundation of Shandong Province (No. ZR2020ZD09), the Natural Science Foundation of Shandong Province (Nos. ZR2020QE063, ZR202108180009, and ZR2023QE059), and the Postdoctoral Program of Qingdao (No. QDBSH20220202019). We express our grateful thanks to them for their financial support.

Declaration of competing interest

All the contributing authors report no conflict of interests in this work.

Author contribution statement

J. K. C.: Data curation, investigation, formal analysis, writing manuscript, methodology, experimental design. G. F. W.: Visualization, data curation, methodology. B. S.: Visualization, conceptualization. Y. Z.: Data curation. M.Y. L.: Validation. L. W.: Resources. G. C. L.: Resources. A. L. M.: Supervision, project administration. S. Q. D.: Project administration, funding acquisition, writing – review & editing. Z. J. L.: Project administration, resources, funding acquisition, writing – review & editing, supervision. All the authors have approved the final manuscript.

Use of AI statement

None.

References

[1] Zhao, Z. M.; Nian, B. B.; Lei, Y. J.; Zhao, L. Y.; Hedhili, M. N.; Guo, D.; Shi, Z. X.; Zhao, W. L.; El-Demellawi, J. K.; Wang, Y. Z. et al. Passivation layers in Mg-metal batteries: Robust interphases for Li-metal batteries. *Adv. Mater.* **2024**, *36*, 2402626.

[2] Liu, Y. H.; Qu, B. H.; Li, S. Y.; Lian, X. J.; Luo, Y. Y.; Shen, X.; Xu, C. H.; Wang, J. F.; Pan, F. S. Recent advances and prospects of chalcogenide cathodes for rechargeable magnesium batteries. *Adv. Funct. Mater.* **2024**, *34*, 2405586.

[3] Li, Y. J.; Feng, X.; Lieu, W. Y.; Fu, L.; Zhang, C.; Ghosh, T.; Thakur, A.; Wyatt, B. C.; Anasori, B.; Liu, W. et al. MXene-based anode-free magnesium metal battery. *Adv. Funct. Mater.* **2023**, *33*, 2303067.

[4] Koketsu, T.; Ma, J. W.; Morgan, B. J.; Body, M.; Legein, C.; Dachraoui, W.; Giannini, M.; Demortiere, A., Salanne, M.; Dardoize, F.; Groult, H. et al. Reversible magnesium and aluminium ions insertion in cation-deficient anatase TiO_2. *Nat. Mater.* **2017**, *16*, 1142–1148.

[5] Shi, H. C.; Wang, G. X.; Wang, Z. C.; Yang, L.; Zhang, S.; Dong, S. M.; Qu, B. H.; Du, A. B.; Li, Z. Y.; Zhou, X. Y. et al. Understanding the cathode-electrolyte interfacial chemistry in rechargeable magnesium batteries. *Adv. Sci.* **2024**, *11*, 2401536.

[6] Tian, Y. X.; Chen, J. K.; Wang, G. F.; Sun, B.; Meng, A. L.; Wang, L.; Li, G. C.; Huang, J. F.; Ding, S. Q.; Li, Z. J. Stable multi-electron reaction stimulated by W doping VS_4 for enhancing magnesium storage performance. *J. Energy Chem.* **2024**, *89*, 89–98.

[7] Sun, R. J.; Jin, S. F.; Deng, J.; Hao, M. N.; Zhong, X.; Ma, Y. X.; Li, M. X.; Chen, X. L. Chemical pressure boost record-high superconductivity in van der waals materials $FeSe_{1-x}S_x$. *Adv. Funct. Mater.* **2021**, *31*, 2102917.

[8] Ding, S. Q.; Dai, X.; Tian, Y. X.; Song, B.; Wang, L.; Li, G. C.; Li, S. X.; Huang, J. F.; Li, Z. J.; Meng, A. L. Insight into the coordinating mechanism of multi-electron reaction and structural stability induced by K^+ pre-intercalation for magnesium ions batteries. *Nano Energy* **2022**, *93*, 106838.

[9] Li, Z. Y.; Vinayan, B. P.; Jankowski, P.; Njel, C.; Roy, A.; Vegge, T.; Maibach, J.; Lastra, J. M. G.; Fichtner, M.; Zhao-Karger, Z. Multi-electron reactions enabled by anion-based redox chemistry for high-energy multivalent rechargeable batteries. *Angew. Chem., Int. Ed.* **2020**, *59*, 11483–11490.

[10] Wang, Y. R.; Liu, Z. T.; Wang, C. X.; Yi, X.; Chen, R. P.; Ma, L. B.; Hu, Y.; Zhu, G. Y.; Chen, T.; Tie, Z. X. et al. Highly branched VS_4 nanodendrites with 1D atomic-chain structure as a promising cathode material for long-cycling magnesium batteries. *Adv. Mater.* **2018**, *30*, 1802563.

[11] Li, X. R.; Shen, Y. L.; Wang, X. Y.; Ni, S.; Yue, L. G.; Khan, S. A.;

Zhao, J. Y.; Xu, J. J. Emerging halides as a new class of high-performance cathodes. *Energy Storage Mater.* **2024**, *71*, 103660.
[12] Li, X. X.; Guo, T. Q.; Shang, Y.; Zheng, T.; Jia, B. B.; Niu, X. G.; Zhu, Y. J.; Wang, Z. C. Interior-confined vacancy in potassium manganese hexacyanoferrate for ultra-stable potassium-ion batteries. *Adv. Mater.* **2024**, *36*, 2310428.
[13] Bi, H. W.; Zhu, S. L.; Liang, Y. Q.; Jiang, H.; Li, Z. Y.; Wu, S. L.; Wei, H.; Chang, C. T.; Wang, H.; Cui, Z. D. Improved ions storage performance for various batteries: Anatase TiO_2 with high-concentration of Ti vacancies. *Mater. Chem. Phys.* **2023**, *301*, 127591.
[14] Chen, F. Y.; Zhao, B. Q.; Huang, K. F.; Ma, X. F.; Li, H. Y.; Zhang, X.; Diao, J.; Yue, J. L.; Huang, G. S.; Wang, J. F. et al. Dual-defect engineering strategy enables high-durability rechargeable magnesium-metal batteries. *Nano-Micro Lett.* **2024**, *16*, 184.
[15] Jiang, R.; Liu, B. L.; Du, C. L.; Jin, M. W.; Liu, X.; Ma, X. L.; Zhu, Y. Q.; Zou, M. S.; Cao, C. B. Microwave-induced defect-rich vanadium sulfide cathodes for highly reversible electrochemical magnesium storage. *Chem. Eng. J.* **2024**, *488*, 150487.
[16] Song, Q. Y.; Zhou, S. H.; Wang, S. Y.; Li, S.; Xu, L.; Qiu, J. X. Insights into the oxygen vacancies in transition metal oxides for aqueous zinc-ion batteries. *Chem. Eng. J.* **2023**, *461*, 142033.
[17] Ding, S. Q.; Dai, X.; Li, Z. J.; Wang, C. S.; Meng, A. L.; Wang, L.; Li, G. C.; Huang, J. F.; Li, S. X. PVP-induced synergistic engineering of interlayer, self-doping, active surface and vacancies in VS_4 for enhancing magnesium ions storage and durability. *Energy Storage Mater.* **2022**, *47*, 211–222.
[18] Luo, C. W.; Cai, L.; Xie, C.; Li, G.; Jiang, T. J. Sulfur vacancies on MoS_2 enhanced the activation of peroxymonosulfate through the co-existence of radical and non-radical pathways to degrade organic pollutants in wastewater. *RSC Adv.* **2022**, *12*, 25364–25376.
[19] Li, Q. Q.; Guo, Y. L.; Tian, Y.; Liu, W. M.; Chu, K. Activating VS_2 basal planes for enhanced NRR electrocatalysis: The synergistic role of S-vacancies and B dopants. *J. Mater. Chem. A* **2020**, *8*, 16195–16202.
[20] Xu, R.; Huang, J. F.; Cao, L. Y.; Feng, L.; Feng, Y. Q.; Kou, L. J.; Liu, Q. Q.; Yang, D.; Feng, L. L. VS_2 microflowers with *in situ* embedded few-layer MoS_2 nanobelts for enhanced hydrogen evolution reaction at high current density. *J. Electrochem. Soc.* **2020**, *167*, 026508.
[21] Ding, S. Q.; Dai, X.; Li, Z. J.; Meng, A. L.; Wang, L.; Li, G. C.; Li, S. X. Strategy of cation/anion co-doping for potential elevating of VS_4 cathode for magnesium ion batteries. *Chem. Eng. J.* **2022**, *439*, 135778.
[22] Liu, Y.; Huang, R. Q.; Wei, N.; Zhou, Y. L. Polydopamine shell-coated hierarchical VS_4 sub-microspheres for enhanced sodium storage. *Ionics* **2023**, *29*, 651–660.
[23] Zhang, Y. X.; Li, J. T.; Li, X. T.; Shan, L. A.; Zhao, W. J.; Wang, J.; Gao, Q.; Cai, Z.; Zhou, C. G.; Han, B.; Amine, K.; Sun, R. M. Electron configuration modulation induced stabilized 1T-MoS_2 for enhanced sodium ion storage. *Nano Lett.* **2024**, *24*, 3331–3338.
[24] Cai, X. Y.; Xu, Y. A.; An, Q. Y.; Jiang, Y. L.; Liu, Z. A.; Xiong, F. Y.; Zou, W. Y.; Zhang, G.; Dai, Y. H.; Yu, R. H. et al. MOF derived TiO_2 with reversible magnesium pseudocapacitance for ultralong-life Mg metal batteries. *Chem. Eng. J.* **2021**, *418*, 128491.
[25] Chen, D.; Zhang, Y. J.; Shen, J. W.; Li, X.; Chen, Z. X.; Cao, S. A.; Li, T.; Xu, F. Facile synthesis and electrochemical Mg-storage performance of Sb_2Se_3 nanowires and Bi_2Se_3 nanosheets. *Dalton Trans.* **2019**, *48*, 17516–17523.
[26] Ding, S. Q.; Tian, Y. X.; Chen, J. K.; Lv, H.; Wang, A. M.; Dai, J. J.; Dai, X.; Wang, L.; Li, G. C.; Meng, A. L. et al. Multidimensional defects tailoring local electron and Mg^{2+} diffusion channels for boosting magnesium storage performance of WO_3/MoO_2. *J. Energy Chem.* **2023**, *84*, 476–485.
[27] Ding, S. Q.; Tian, Y. X.; Chen, J. K.; Wang, G. F.; Sun, B.; Lv, H.; Wang, L.; Li, G. C.; Meng, A. L.; Li, Z. J. Crystalline@amorphous core-shell structure of WO_3@$WO_{3-x}S_x$ established via doping strategy for enhancing magnesium ions storage performance. *J. Magnesium Alloys*, in press, DOI: 10.1016/j.jma.2024.04.029.
[28] Shi, M. Y.; Li, T. L.; Shang, H.; Huang, T. L.; Miao, Y. D.; Zhang, C. C.; Qi, J. Q.; Wei, F. X.; Xiao, B.; Xu, H. et al. Electronic structure engineering on $NiSe_2$ micro-octahedra via nitrogen doping enabling long cycle life magnesium ion batteries. *J. Colloid Interface Sci.* **2023**, *645*, 850–859.
[29] Xia, Y. P.; Chen, C. X.; Ran, L.; Zhang, H. A.; Cui, S.; Xiao, P. F.; Xu, F.; Zhang, D. H.; Li, T. Preferentially *in-situ* generated copper nanograins boosting fast kinetic conversion magnesium storage of bimetallic copper-cobalt sulfide cathode. *Chem. Eng. J.* **2024**, *488*, 151133.
[30] Zhang, Y. M.; Li, D. D.; Li, J. Z.; Li, Y. L.; Wang, L. L.; Xu, H.; Han, W. Flexible TiVCT$_x$ MXene film for high-performance magnesium-ion storage device. *J. Colloid Interface Sci.* **2024**, *657*, 550–558.
[31] Zhang, Y. J.; Li, T.; Cao, S. A.; Luo, W.; Xu, F. Cu_2MoS_4 hollow nanocages with fast and stable Mg^{2+}-storage performance. *Chem. Eng. J.* **2020**, *387*, 124125.